Brief Communications

Motor Cortex Layer V Pyramidal Neurons Exhibit Dendritic Regression, Spine Loss, and Increased Synaptic Excitation in the Presymptomatic hSOD1^{G93A} Mouse Model of Amyotrophic Lateral Sclerosis

Matthew J. Fogarty,[1] Peter G. Noakes,[1,2]* and Mark C. Bellingham[1]*

[1]School of Biomedical Sciences, [2]Queensland Brain Institute, University of Queensland, St. Lucia, Queensland 4072, Australia

Motor cortex layer V pyramidal neurons (LVPNs) regulate voluntary control of motor output and selectively degenerate (along with lower motor neurons) in amyotrophic lateral sclerosis. Using dye-filling and whole-cell patch clamping in brain slices, together with high-resolution spinning disk confocal *z*-stack mosaics, we characterized the earliest presymptomatic cortical LVPN morphologic and electrophysiological perturbations in hSOD1^{G93A} (SOD1) mice to date. Apical dendritic regression occurred from postnatal day (P) 28, dendritic spine loss from P21, and increased EPSC frequency from P21 in SOD1 LVPNs. These findings demonstrate extensive early changes in motor cortex of the SOD1 mouse model, which thus recapitulates clinically relevant cortical pathophysiology more faithfully than previously thought.

Key words: **motor neuron disease**

Introduction

Amyotrophic lateral sclerosis (ALS) is a progressive neurodegenerative disorder clinically characterized by loss of upper motor neurons of the motor cortex and corticospinal tract, including layer V pyramidal neurons (LVPNs) and loss of brainstem and spinal cord lower motor neurons (MNs), causing muscle weakness and death within 3–4 years from onset (Turner et al., 2013). Cu/Zn-superoxide dismutase (SOD1) mutations in familial ALS (Rosen et al., 1993) have provided key pathogenic insights into ALS, through the use of transgenic mice overexpressing the mutant human hSOD1^{G93A} gene, which exhibit progressive MN degeneration resembling human ALS (Gurney et al., 1994).

Although ALS is an adult-onset disease, pathogenic lower MN changes in the SOD1 model occur from late embryogenesis onwards (van Zundert et al., 2008; Vinsant et al., 2013). Studies of SOD1 models have largely focused on understanding lower MN and peripheral nervous system pathology, overlooking important cortical and subcortical clinical features of human ALS (Turner et al., 2013).

Clinically, motor cortex LVPNs are reduced in ALS (Mochizuki et al., 2011). Golgi-impregnated human LVPNs show dendritic degeneration, "stumped" apical dendrites that do not reach the pia, dendritic spine loss and somatic swellings (Hammer et al., 1979). In addition, cortical hyperexcitation, proposed as a key determinant in clinical progression (Bae et al., 2013), may occur before clinical symptoms (Vucic et al., 2008) and separates ALS from other neuromotor disorders (Vucic et al., 2011). Support for cortical involvement in the etiology of human ALS comes from clinical observations that brainstem and spinal motor nuclei without direct cortical connections (oculomotor, abducens, and Onuf's nuclei) are relatively spared during the disease (Eisen et al., 1992).

In the mutant SOD1 mouse model, corticospinal neurons (a type of LVPN) display somatic abnormalities at postnatal day (P) 30 (Ozdinler et al., 2011) with cell loss, autophagic apical dendrite degeneration, and spine loss by P60 (Jara et al., 2012). Additionally, cortical cultures from SOD1 mice show intrinsic hyperexcitability (Pieri et al., 2009).

This study aimed to determine the extent and timing of dendritic degeneration and nature of LVPN functional synaptic inputs at presymptomatic ages P21–P27, beginning after rapid increases in cortical volume and connectivity have plateaued (Bahrey and Moody, 2003; Ingalhalikar et al., 2014), and P28–P40, beginning with the earliest reported motor behavior defects and muscle denervation at P28 (Vinsant et al., 2013) and ending when corticospinal neuron loss begins (Ozdinler et al., 2011). Using dye-filling and whole-cell patch clamping in conjunction with spinning disk confocal neuronal imaging, we report early regression of LVPN dendritic arbors and spines, along with si-

Received Aug. 20, 2014; revised Oct. 21, 2014; accepted Nov. 10, 2014.

Author contributions: M.J.F., P.G.N., and M.C.B. designed research; M.J.F. performed research; M.J.F. and M.C.B. analyzed data; M.J.F., P.G.N., and M.C.B. wrote the paper.

The work was supported by grants to M.C.B. and P.G.N. (National Health and Medical Research Council Project Grant 1065884 and Motor Neuron Disease Research Institute Australia). We thank Dr. S. Ngo for providing experimental animals, M. Shayegh and M. White for genotyping, and L. Hammond and Dr. D. Matthews for microscopy assistance (Australia Research Council Linkage Infrastructure, Equipment and Facilities Grant LE100100074).

The authors declare no competing financial interests.

*P.G.N. and M.C.B. contributed equally to this study.

Correspondence should be addressed to Mark C. Bellingham, School of Biomedical Sciences, University of Queensland, St. Lucia, Queensland 4072, Australia. E-mail. mark.bellingham@uq.edu.au.

DOI:10.1523/JNEUROSCI.3483-14.2015

 0270-6474/15/350643-05$15.00/0

multaneous increases in functional excitatory neurotransmission. Our findings suggest that excessive spontaneous synaptic excitatory neurotransmission in the motor cortex is correlated with dendritic regression of LVPNs before neuronal death and other ALS-like symptoms.

Materials and Methods

Mice. A total of 16 male and 25 female age-matched and litter-matched wild-type (WT) and heterozygous transgenic mice overexpressing the hSOD1^{G93A} mutation were used. The percentage of WT and SOD1 males was similar for each age studied (P21–P27, 33%; P28–P40, ~42%). All procedures were approved by The University of Queensland Animal Ethics Committee and complied with national ethical guidelines.

Slice preparations. Mice were anesthetized with sodium pentobarbitone (60–80 mg/kg, i.p.; Vetcare) and decapitated. During dissection, the tissue was bathed in ice-cold high-Mg^{2+} Ringer's solution containing the following (in mM): 130 NaCl, 3 KCl, 26 $NaHCO_3$, 1.25 NaH_2PO_4, 5 $MgCl_2$, 1 $CaCl_2$, and 10 D-glucose. Ringer's solutions were continuously bubbled with 95% O_2/5% CO_2 to maintain pH at 7.4. Off-coronal slices (300 μm) with a 15° rostral rotation containing motor cortex were cut using a vibratome (Leica VT 1200S, Leica Biosystems). Slices were incubated for 60 min in high-Mg^{2+} Ringer's solution warmed to 34°C and then moved to a normal Ringer's (1 mM $MgCl_2$, 2 mM $CaCl_2$) solution maintained at 22°C for 30 min before start of recording and labeling.

Electrophysiology. Patch electrodes were pulled from borosilicate glass capillaries (Edwards Medical) giving a tip resistance of 3–4 MΩ and filled with intracellular solution containing the following (in mM): 135 Cs^+MeSO_4, 6 KCl, 1 EGTA, 2 $MgCl_2$, 5 Na-HEPES, 3 ATP-Mg^{2+}, 0.3 GTP-Tris, pH 7.25 (osmolarity, 305 ± 5 mOsm; Kanjhan and Bellingham, 2013). The pipette was then back-filled with 1–2 μl of intracellular solution containing 2% Neurobiotin (NB; Vector Laboratories). A single brain slice was stabilized with a metal mesh in a tissue chamber on a Nikon E600FN microscope fitted with infrared-differential interference contrast optics, continuously superfused (1–2 ml/min) with normal Ringer's solution at 22°C, and viewed on a monitor through a 60× water-immersion objective and an infrared video camera (Hamamatsu). Recordings and voltage pulse protocols were made with an Axopatch 1D amplifier (Molecular Devices). Data were sampled at 10 kHz and low-pass filtered at 2 kHz using PClamp 10.2 software and a Digidata 1332A digitizer (Molecular Devices). A patch electrode was advanced toward visually identified LVPNs in the motor cortex with a micromanipulator (Sutter Instrument). Gentle suction was applied until a stable seal of ~300–1000 MΩ was obtained. The NB electroporation procedure was modified from that described for brainstem MNs. Square-wave voltage steps (0.5 s, 1 Hz) of 5–25 mV that generated current pulses of 300–500 pA were applied for 3–5 min. If the membrane seal was ruptured by voltage pulses or suction, spontaneous IPSCs and EPSCs were recorded at holding membrane potentials of 0 mV and −70 mV respectively. Spontaneous synaptic events were detected over 75 s of continuous recording, chosen randomly from 2 min epochs, using Axograph X (Axograph Scientific). Peak-to-peak noise ranged from 2 to 10 pA, and only events with peak amplitudes of >2× half peak-to-peak noise were analyzed.

Immunocytochemistry and imaging. After filling, slices were left in the bath for >5 min to allow NB diffusion, then fixed in 4% paraformaldehyde in 0.1 M PBS for 30 min, washed in PBS and incubated for 4 h in PBS containing 4% bovine serum albumin (BSA) and 0.05% Triton X-100 at 4°C. Slices were then incubated for 4 h at 4°C in Cy3-streptavidin (Sigma-Aldrich; 1:500 in 4% BSA PBS) to visualize NB. Slices were washed in PBS and mounted on slides. High-resolution 60× water-immersion objective mosaic *z*-stacks (0.33 μm *z*-steps) of LVPNs were captured using a W1 Yokogawa spinning disk confocal scanner (Yokogawa Electric) equipped with a Flash 4.0 scientific complementary metal-oxide semiconductor camera (Hamamatsu).

Morphologic quantification. Morphological properties of NB-filled LVPNs were analyzed from confocal images using Neurolucida (MBF Bioscience). Dendrites were divided into apical or basal; small processes were classified as spines only if they were <3 μm long and <0.8 μm in cross-sectional diameter (Harris, 1999). A total LVPN dendrite length of 222,602 μm was traced for length and spine density in 44 individual LVPNs.

Statistical analysis. Data were analyzed with Prism 6 (Graphpad) and expressed as mean ± SE. Statistically significant differences were determined using two-way ANOVAs with Bonferroni's post-test, where $^*p < 0.05$, $^{**}p < 0.01$, $^{***}p < 0.001$, and $^{****}p < 0.0001$ were statistically significant. A power analysis (GPower3; Faul et al., 2007) showed that sample size could detect an effect size of 0.25 with $p > 0.8$.

Results

Regression of apical dendritic arbor length in SOD1 LVPNs

The elongated apical and short basal dendritic structure of motor cortex LVPNs facilitate integration of divergent sources of synaptic inputs to produce coordinated motor outputs. Changes in LVPN dendritic structure are therefore likely to affect synaptic transmission onto the LVPN and compromise neuromotor function. To assess dendritic arborization in LVPNs of WT and SOD1 mice, we studied LVPN morphology at two developmental stages in presymptomatic SOD1 mice and in age-matched and litter-matched WT controls: P21–P27, after the end of rapid functional and morphological cortical maturation (Bahrey and Moody, 2003; Ingalhalikar et al., 2014), and P28–P40 (Fig. 1*A*,*B*), after the onset of hindlimb motor weakness and muscle denervation (Vinsant et al., 2013).

Total LVPN dendritic length was unchanged at P21–P27 (WT, 4864 ± 450 μm, $n = 6$; SOD1, 3580 ± 623 μm, $n = 9$; $p = 0.31$; Fig. 1*G*). By lower MN symptom onset at P28–P40, SOD1 LVPN dendritic arbors decreased by 31% compared with WT (WT, 6622 ± 418 μm, $n = 14$; SOD1, 4566 ± 479 μm, $n = 15$; $^{**}p = 0.0044$; Fig. 1*G*). Mean LVPN apical arbor length was unchanged at P21–P27 (WT, 3122 ± 521 μm, $n = 6$; SOD1, 1693 ± 624 μm, $n = 9$; $p = 0.10$; Fig. 1*H*). By P28–P40, SOD1 LVPN apical arbors were decreased by 49% compared with WT (WT, 3951 ± 354 μm, $n = 14$; SOD1, 2028 ± 379 μm, $n = 15$; $^{***}p = 0.0009$; Fig. 1*H*). Mean LVPN apical terminal distance from soma was unchanged at P21–P27 (WT, 724 ± 40 μm, $n = 6$; SOD1, 492 ± 93 μm, $n = 9$; $p = 0.16$). By P28–P40, SOD1 LVPN apical terminal distances from the soma were decreased by 33% compared with WT (WT, 762 ± 52 μm, $n = 14$; SOD1, 511 ± 77 μm, $n = 15$; $^*p = 0.017$). By contrast, LVPN basal arbor length was unchanged at both P21–P27 (WT, 2290 ± 327 μm, $n = 6$; SOD1, 1497 ± 366 μm, $n = 9$; $p = 0.61$) and P28–P40 (WT, 2930 ± 444 μm, $n = 14$; SOD1, 2691 ± 407 μm, $n = 15$; $p > 0.99$). There was no difference in LVPN soma size between SOD1 and WT at P21–P27 (WT, 1570 ± 379 μm^3, $n = 6$; SOD1, 1588 ± 161 μm^3, $n = 9$; $p > 0.99$) and P28–P40 (WT, 2273 ± 255 μm^3, $n = 14$; SOD1, 1979 ± 204 μm^3, $n = 15$; $p = 0.68$; but see Ozdinler et al., 2011; Jara et al., 2012).

These observations suggest that LVPN apical dendritic arbors in the motor cortex undergo selective recession at presymptomatic stages of the SOD1 mouse model. This recession was clearly evident at P28–P40, when muscle denervation has begun, but before lower MN loss at P35–P60 (Ngo et al., 2012; Vinsant et al., 2013). Apical dendrite "degeneration" of identified corticospinal neurons has previously been reported in SOD1 mice at P60. Our data show striking shrinkage in SOD1 LVPN dendritic arbors by P28 and continuing to P40, due to reduction in apical dendrite length, both in extent to the pia and in decreased apical collateral branch length and number.

Decreased apical and basal spine densities in SOD1 LVPNs

A reduction in the apical dendritic arbor of SOD1 LVPNs could alter the number of presynaptic inputs onto these neurons. Ex-

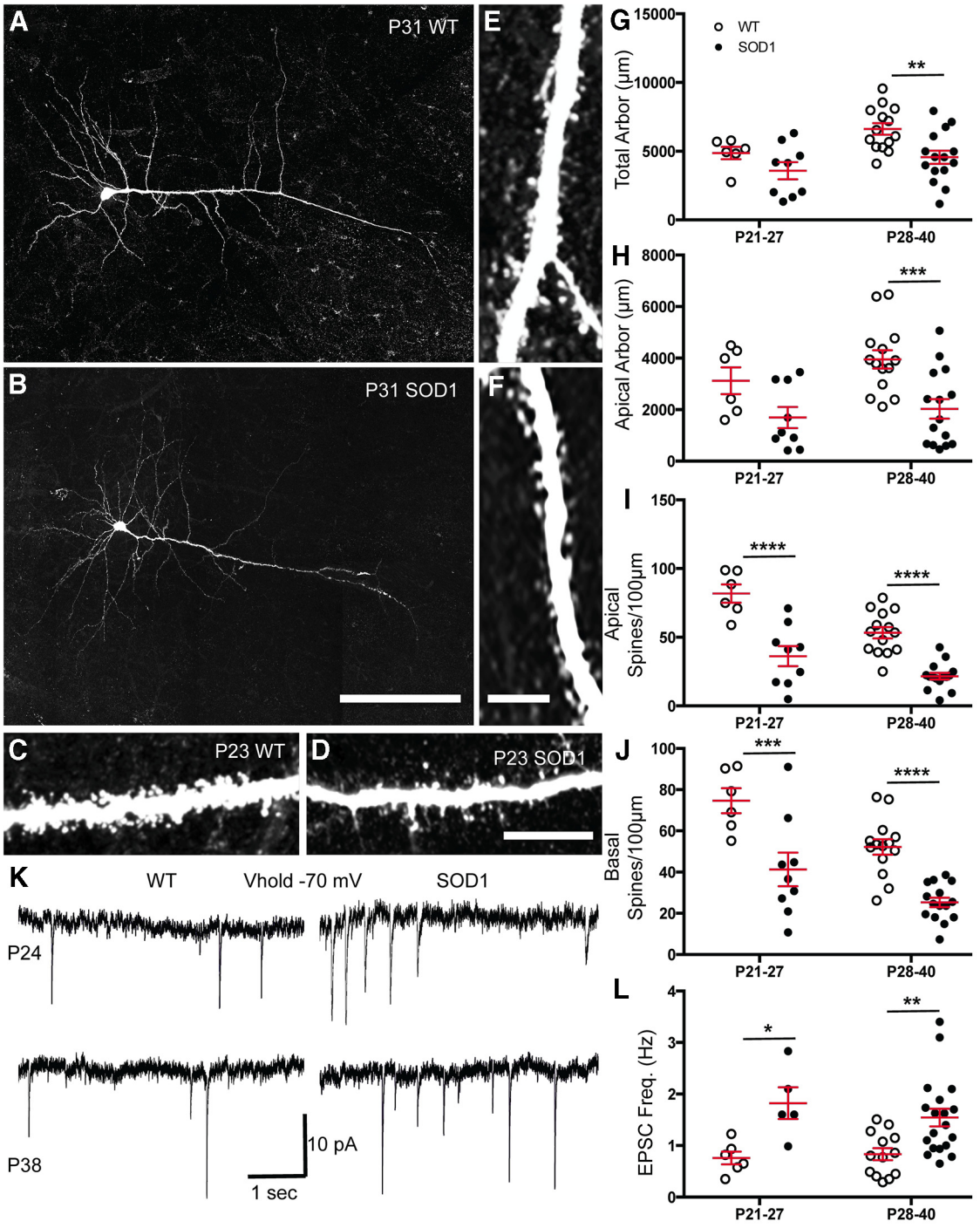

Figure 1. Apical dendritic regression, spine loss, and increased EPSC frequency occurs in motor cortex LVPNs of presymptomatic SOD1 mice. ***A***, ***B***, Dendritic arbors of NB-filled LVPNs within primary motor cortex from WT (***A***) and SOD1 (***B***) mice. ***C–F***, LVPNs show decreased apical dendritic spines in P23 and P31 SOD1 mice compared with age-matched and litter-matched WT mice. ***G–J***, Scatterplots of morphological measurements in P21–P27 and P28 –P40 SOD1 and WT LVPNs, showing decreased total dendritic arbor length in P28 –P40 SOD1 LVPNs (***G***), decreased apical dendritic arbor length in P28 –P40 SOD1 LVPNs (***H***), and decreased dendritic spine densities per 100 μm apical and basal dendrite respectively in both P21–P27 and P28 –P40 SOD1 LVPNs (***I***, ***J***). ***K***, Representative electrophysiology traces showing increased EPSC frequency at −70 mV holding voltage in SOD1 LVPN at ages P24 and P38. ***L***, Scatterplot showing increased EPSC frequency in both P21–P27 and P28 –P40 SOD1 LVPNs compared with WT. Two-way ANOVA with Bonferroni's post-test; $^{*}p < 0.05$, $^{**}p < 0.01$, $^{***}p < 0.001$, and $^{****}p < 0.0001$. For morphology: WT, $n = 6$ (P21–P27) and $n = 14$ (P28 –P40); SOD1, $n = 9$ (P21–P27) and $n = 15$ (P28 –P40); For EPSCs: WT, $n = 6$ (P21–P27) and $n = 13$ (P28 –P40); SOD1, $n = 5$ (P21–P27) and $n = 19$ (P28 –P40). Scale bars: ***A***, ***B***, 250 μm; ***C–F***, 5 μm.

citatory presynaptic inputs to LVPNs are usually associated with dendritic spines (Spruston, 2008; Yu and Zuo, 2011). We therefore examined morphological spine density in motor cortex LVPNs from SOD1 mice and their age-matched littermates by quantifying the number of spines per 100 μm length of dendrite in both apical and basal dendritic LVPN trees. The mean apical dendritic spine density decreased by 56% at P21–P27 (WT, 81.8 ± 6.6, $n = 6$; SOD1, 36.2 ± 7.3, $n = 9$; $^{****}p < 0.0001$; Fig. 1*C*,*D*,*I*) and by 59% at P28 –P40 (WT, 53.3 ± 4.1, $n = 14$; SOD1, 21.6 ± 2.5, $n = 15$; $^{****}p < 0.0001$; Fig. 1*E*,*F*,*I*). The mean basal dendritic spine density also decreased by 45% at P21–P27 (WT, 74.6 ± 6.1, $n = 6$; SOD1, 41.3 ± 8.2, $n = 9$; $^{***}p = 0.009$; Fig. 1*J*)

and by 52% at P28–P40 (WT, 52.2 ± 3.7, $n = 14$; SOD1, 25.3 ± 2.3, $n = 15$; $^{****}p < 0.0001$; Fig. 1*J*).

These data suggest that postsynaptic alterations occur in motor cortex LVPNs as early as P21 and that loss of spines occurs across the entire dendritic arbor. Spine reductions in apical, but not basal, dendrites of corticospinal neurons have been previously reported in P60 SOD1 mice (Jara et al., 2012).

Increased frequency of spontaneous excitatory neurotransmission in SOD1 LVPNs

Spine density reductions associated with glutamate-induced excitotoxicity have been described for decades (Olney, 1971) and spine and/or synaptic dysfunction may precede neuronal cell death in many neurodegenerative diseases (Luebke et al., 2010), including the SOD1 model of ALS (van Zundert et al., 2008). As glutamate is the most abundant excitatory neurotransmitter and excitatory synaptic activity is a potent regulator of dendrite and spine dynamics (Yu and Zuo, 2011), we quantified excitatory and inhibitory synaptic activity in motor cortex LVPNs, using whole-cell patch-clamp recordings from presymptomatic SOD1 and age-matched littermate controls, for P21–P27 and P28–P40 age groups.

At −70 mV, all spontaneous inward currents were excitatory. The mean frequency of spontaneous EPSCs in SOD1 LVPNs increased by 141% at P21–27 (WT, 0.76 ± 0.12 Hz, $n = 6$; SOD1, 1.82 ± 0.31 Hz, $n = 5$; $^{*}p = 0.013$; Fig. 1*K*,*L*, top row) and by 85% at P28–P40 (WT, 0.83 ± 0.12 Hz, $n = 13$; SOD1, 1.54 ± 0.17 Hz, $n = 19$; $^{**}p = 0.005$; Fig. 1*K*,*L*, bottom row). By contrast, EPSC shape parameters (10–90% rise time, amplitude, and half-width) and LVPN electrophysiological parameters remained unchanged across the two genotypes over the two age groups. The mean EPSC shape and electrophysiological parameters were as follows: (1) 10–90% rise time (P21–P27: WT, 3.0 ± 0.7 ms, $n = 6$; SOD1, 3.8 ± 1.2 ms, $n = 5$; $p > 0.99$; P28–P40: WT, 2.9 ± 0.4 ms, $n = 13$; SOD1, 3.1 ± 0.5 ms, $n = 19$; $p > 0.99$), (2) amplitude (P21–P27: WT, − 30.6 ± 9.2 pA, $n = 6$; SOD1, −26.1 ± 7.2 pA, $n = 5$; $p > 0.99$; P28–P40: WT, −16.6 ± 3.0 pA, $n = 13$; SOD1, −18.9 ± 2.4 pA, $n = 19$; $p > 0.99$), and (3) half-width (P21–P27: WT, 4.2 ± 0.9 ms, $n = 6$; SOD1, 6.1 ± 1.0 ms, $n = 5$; $p = 0.58$; P28–P40: WT, 4.9 ± 0.9 ms, $n = 13$; SOD1, 4.0 ± 0.7 ms, $n = 19$; $p = 0.35$); (4) membrane capacitance (P21–P27: WT, 22 ± 3 pS, $n = 6$; SOD1, 28 ± 4 pS, $n = 5$; $p = 0.55$; P28–P40: WT, 32 ± 2 ms, $n = 13$; SOD1, 26 ± 2 ms, $n = 19$; $p = 0.06$); and (5) holding current at −70 mV (P21–P27: WT, −208 ± 129 pA, $n = 6$; SOD1, −21 ± 10 pA, $n = 5$; $p = 0.09$; P28–P40: WT, −174 ± 38 pA, $n = 13$; SOD1, −70 ± 22 pA, $n = 19$; $p = 0.12$).

At 0 mV, all spontaneous outward currents were inhibitory. There were no differences between SOD1 and WT LVPN IPSC parameters at all ages studied, including IPSC frequency, 10–90% rise time, amplitude, and half-width. The mean IPSC parameters were as follows: (1) frequency (P21–P27: WT, 2.45 ± 0.49 Hz, $n = 6$; SOD1, 2.47 ± 0.40 Hz, $n = 7$; $p > 0.99$; P28–P40: WT, 2.37 ± 0.25 Hz, $n = 14$; SOD1, 1.52 ± 0.22 Hz, $n = 20$; $p = 0.21$); (2) 10–90% rise time (P21–P27: WT, 3.5 ± 0.7 ms, $n = 6$; SOD1, 5.6 ± 1.7 ms, $n = 7$; $p = 0.26$; P28–P40: WT, 3.5 ± 0.6 ms, $n = 14$; SOD1, 4.3 ± 0.4 ms, $n = 20$; $p = 0.68$); (3) amplitude (P21–P27: WT, 13.4 ± 2.9 pA, $n = 6$; SOD1, 12.3 ± 3.8 pA, $n = 7$; $p > 0.99$; P28–P40: WT, 14.3 ± 2.0 pA, $n = 14$; SOD1, 11.8 ± 1.8 pA, $n = 20$; $p = 0.74$), and (3) half-width (P21–P27: WT, 9.2 ± 3.1 ms, $n = 6$; SOD1, 6.3 ± 1.2 ms, $n = 7$; $p = 0.36$; P28–P40: WT, 7.6 ± 0.8 ms, $n = 14$; SOD1, 7.7 ± 0.8 ms, $n = 20$; $p > 0.99$).

Together, our patch-clamp data suggest motor cortex LVPNs of SOD1 mice receive increased excitatory neurotransmission as early as P21, without compensatory increases in inhibitory neurotransmission. This may lead to glutamate-induced excitotoxicity, recognized as one of the main pathogenic triggers of ALS and other neurodegenerative disorders (Bogaert et al., 2010).

Discussion

Selective degeneration of both upper and lower MNs is pathognomonic for ALS. While lower MN loss and dysfunction have been increasingly well characterized in animal models of ALS (Gurney et al., 1994; van Zundert et al., 2008; Ngo et al., 2012; Vinsant et al., 2013; Delestrée et al., 2014), there have been few investigations of cortical changes in these models (Pieri et al., 2009; Ozdinler et al., 2011; Jara et al., 2012). The morphological and electrophysiological changes reported here strongly support the early onset of motor cortical dysfunction in the SOD1 mouse model of ALS. Changes are evident from P21, persist up to the onset of LVPN loss from P35 (Ozdinler et al., 2011), and precede the onset of lower MN symptoms from P28 onwards (Vinsant et al., 2013) and, according to previous reports, the onset of apical dendrite regression and spine loss in corticospinal neurons at P60 (Jara et al., 2012).

While we have not identified the projection target of the LVPNs recorded here, our sample is highly likely to contain corticospinal neurons, as >45% of motor cortex LVPNs are retrogradely labeled by spinal tracer injection (Brecht et al., 2013). We found a significant decline in both apical and basal dendritic spine density of SOD1 LVPNs from P21, 3–5 weeks earlier than previously reported in apical (but not basal) dendrites of SOD1 corticospinal neurons (Jara et al., 2012). Dendritic loss in SOD1 LVPNs was confined to apical dendrites, both in reduced extension of the apical dendrite toward the pia and reduction in the oblique apical branches within layer II/III. Both spine loss and dendrite regression occurred before symptom onset and corticospinal neuron loss. These observations in hSOD1^{G93A} mice are consistent with the selective vulnerability of cortical neurons in ALS seen in human pathology (Hammer et al., 1979).

Pyramidal neurons, such as LVPNs, are typically covered with thousands of dendritic spines, predominantly constituting the postsynaptic domains of glutamatergic synapses (Spruston, 2008). Apical dendritic spines of motor cortex LVPNs receive excitatory inputs from thalamocortical neurons and from local and contralateral layer II/III neurons (Jara et al., 2012; Brecht et al., 2013; Hooks et al., 2013). Basal dendritic spines preferentially receive excitatory inputs from thalamic sensory and motor nuclei and from secondary motor cortex (Hooks et al., 2013). We saw increased functional excitatory synaptic activity onto SOD11 LVPNs, compared with controls, at all ages studied. By contrast, inhibitory synaptic activity in LVPNs was unchanged. Increased EPSC activity and excessive glutamate release is consistent with decreased spine density (Hasbani et al., 2001) and with excitotoxicity as a key etiological driver in ALS (Bogaert et al., 2010; Turner et al., 2013).

It is intriguing that increased EPSC activity has previously been shown in developing lower MNs from SOD1 mice (van Zundert et al., 2008). Our results support the possibility that one factor underlying increased synaptic activity in lower MNs may be increased activity in LVPNs, which regulate lower MN activity via projections to the brainstem and spinal cord. Alternatively, increased glutamate release at synapses made onto LVPNs and onto lower MNs may be a common pathological process leading to their demise in ALS.

Our observation that dendritic spine loss correlated with increased EPSC frequency in SOD1 LVPNs was surprising, as dendritic spines are considered a canonical part of excitatory synapses (Spruston, 2008). However, cultured cortical neurons remain in synaptic contact with one another even after glutamate receptor-induced spine loss (Hasbani et al., 2001). Alternatively,

spine loss may trigger functional compensation by LVPNs, such as increased persistent inward currents, a feature of presymptomatic *in vitro* SOD1 cortical neurons (Pieri et al., 2009), to amplify remaining synaptic inputs (Heckman et al., 2008).

Taken in total, our results demonstrate presymptomatic alterations in SOD1 LVPN dendritic arbors, spine density, and spontaneous synaptic inputs that are evident at P21 and are maintained until P40, when corticospinal neuron loss has begun (Ozdinler et al., 2011). These findings suggest that corticospinal neuron death in the hSOD1^{G93A} model of ALS is preceded by presymptomatic cellular alterations that are likely to cause extensive perturbations of the motor cortex neural network. We note that the presence of direct corticospinal inputs to MNs clearly differs between species. Primates (including humans) have varying levels of direct inputs, ranging from strong for distal hand muscles to weak for proximal limb muscles (for review, see Lemon, 2008). By contrast, functional direct corticospinal inputs to forelimb MNs are lacking in mouse (Alstermark and Ogawa, 2004), although some morphological evidence exists for direct corticospinal contacts on mouse lumbar MNs (Bareyre et al., 2005). Despite these species differences, our demonstration that morphological and functional changes in mouse LVPNs occur before, or are synchronous with, lower MN loss, suggests that direct corticospinal connections may be less important in ALS pathogenesis than previously thought. These changes in the motor cortex of hSOD1^{G93A} mice increase the parallels between this model and well established upper and lower MN symptoms evident in clinical ALS (Vucic et al., 2011), suggesting that the hSOD1^{G93A} mouse will be useful for investigation of the mechanisms and exact chronology of cortical degeneration in ALS.

References

Alstermark B, Ogawa J (2004) In vivo recordings of bulbospinal excitation in adult mouse forelimb motoneurons. J Neurophysiol 92:1958–1962. CrossRef Medline

Bae JS, Simon NG, Menon P, Vucic S, Kiernan MC (2013) The puzzling case of hyperexcitability in amyotrophic lateral sclerosis. J Clin Neurol 9:65–74. CrossRef Medline

Bahrey HL, Moody WJ (2003) Voltage-gated currents, dye and electrical coupling in the embryonic mouse neocortex. Cereb Cortex 13:239–251. CrossRef Medline

Bareyre FM, Kerschensteiner M, Misgeld T, Sanes JR (2005) Transgenic labeling of the corticospinal tract for monitoring axonal responses to spinal cord injury. Nat Med 11:1355–1360. CrossRef Medline

Bogaert E, d'Ydewalle C, Van Den Bosch L (2010) Amyotrophic lateral sclerosis and excitotoxicity: from pathological mechanism to therapeutic target. CNS Neurol Disord Drug Targets 9:297–304. CrossRef Medline

Brecht M, Hatsopoulos NG, Kaneko T, Shepherd GM (2013) Motor cortex microcircuits. Front Neural Circuits 7:196. CrossRef Medline

Delestrée N, Manuel M, Iglesias C, Elbasiouny SM, Heckman CJ, Zytnicki D (2014) Adult spinal motoneurones are not hyperexcitable in a mouse model of inherited amyotrophic lateral sclerosis. J Physiol 592:1687–1703. CrossRef Medline

Eisen A, Kim S, Pant B (1992) Amyotrophic lateral sclerosis (ALS): a phylogenetic disease of the corticomotoneuron? Muscle Nerve 15:219–224. CrossRef Medline

Faul F, Erdfelder E, Lang AG, Buchner A (2007) G*Power 3: a flexible statistical power analysis program for the social, behavioral, and biomedical sciences. Behav Res Methods 39:175–191. CrossRef Medline

Gurney ME, Pu H, Chiu AY, Dal Canto MC, Polchow CY, Alexander DD, Caliendo J, Hentati A, Kwon YW, Deng HX (1994) Motor neuron degeneration in mice that express a human Cu, Zn superoxide dismutase mutation. Science 264:1772–1775. CrossRef Medline

Hammer RP Jr, Tomiyasu U, Scheibel AB (1979) Degeneration of the human Betz cell due to amyotrophic lateral sclerosis. Exp Neurol 63:336–346. CrossRef Medline

Harris KM (1999) Structure, development, and plasticity of dendritic spines. Curr Opin Neurobiol 9:343–348. CrossRef Medline

Hasbani MJ, Schlief ML, Fisher DA, Goldberg MP (2001) Dendritic spines lost during glutamate receptor activation reemerge at original sites of synaptic contact. J Neurosci 21:2393–2403. Medline

Heckman CJ, Hyngstrom AS, Johnson MD (2008) Active properties of motoneurone dendrites: diffuse descending neuromodulation, focused local inhibition. J Physiol 586:1225–1231. CrossRef Medline

Hooks BM, Mao T, Gutnisky DA, Yamawaki N, Svoboda K, Shepherd GM (2013) Organization of cortical and thalamic input to pyramidal neurons in mouse motor cortex. J Neurosci 33:748–760. CrossRef Medline

Ingalhalikar M, Parker D, Ghanbari Y, Smith A, Hua K, Mori S, Abel T, Davatzikos C, Verma R (2014) Connectome and maturation profiles of the developing mouse brain using diffusion tensor imaging. Cereb Cortex. Advance online publication. Retrieved November 15, 2014. Medline

Jara JH, Villa SR, Khan NA, Bohn MC, Ozdinler PH (2012) AAV2-mediated retrograde transduction of corticospinal motor neurons reveals initial and selective apical dendrite degeneration in ALS. Neurobiol Dis 47:174–183. CrossRef Medline

Kanjhan R, Bellingham MC (2013) Neurobiotin electroporation for combined structural and functional analysis of neurons in developing mouse brain slices. In: Excitation and inhibition of neural responses (Pilowsky PM, Farnham MMJ, Fong AY, eds), pp 151–165. New York: Humana.

Lemon RN (2008) Descending pathways in motor control. Annu Rev Neurosci 31:195–218. CrossRef Medline

Luebke JI, Weaver CM, Rocher AB, Rodriguez A, Crimins JL, Dickstein DL, Wearne SL, Hof PR (2010) Dendritic vulnerability in neurodegenerative disease: insights from analyses of cortical pyramidal neurons in transgenic mouse models. Brain Struct Funct 214:181–199. CrossRef Medline

Mochizuki Y, Mizutani T, Shimizu T, Kawata A (2011) Proportional neuronal loss between the primary motor and sensory cortex in amyotrophic lateral sclerosis. Neurosci Lett 503:73–75. CrossRef Medline

Ngo ST, Baumann F, Ridall PG, Pettitt AN, Henderson RD, Bellingham MC, McCombe PA (2012) The relationship between Bayesian motor unit number estimation and histological measurements of motor neurons in wild-type and SOD1(G93A) mice. Clin Neurophysiol 123:2080–2091. CrossRef Medline

Olney JW (1971) Glutamate-induced neuronal necrosis in the infant mouse hypothalamus. An electron microscopic study. J Neuropathol Exp Neurol 30:75–90. CrossRef Medline

Ozdinler PH, Benn S, Yamamoto TH, Güzel M, Brown RH Jr, Macklis JD (2011) Corticospinal motor neurons and related subcerebral projection neurons undergo early and specific neurodegeneration in hSOD1^{G93A} transgenic ALS mice. J Neurosci 31:4166–4177. CrossRef Medline

Pieri M, Carunchio I, Curcio L, Mercuri NB, Zona C (2009) Increased persistent sodium current determines cortical hyperexcitability in a genetic model of amyotrophic lateral sclerosis. Exp Neurol 215:368–379. CrossRef Medline

Rosen DR, Siddique T, Patterson D, Figlewicz DA, Sapp P, Hentati A, Donaldson D, Goto J, O'Regan JP, Deng HX (1993) Mutations in Cu/Zn superoxide dismutase gene are associated with familial amyotrophic lateral sclerosis. Nature 362:59–62. CrossRef Medline

Spruston N (2008) Pyramidal neurons: dendritic structure and synaptic integration. Nat Rev Neurosci 9:206–221. CrossRef Medline

Turner MR, Hardiman O, Benatar M, Brooks BR, Chio A, de Carvalho M, Ince PG, Lin C, Miller RG, Mitsumoto H, Nicholson G, Ravits J, Shaw PJ, Swash M, Talbot K, Traynor BJ, Van den Berg LH, Veldink JH, Vucic S, Kiernan MC (2013) Controversies and priorities in amyotrophic lateral sclerosis. Lancet Neurol 12:310–322. CrossRef Medline

van Zundert B, Peuscher MH, Hynynen M, Chen A, Neve RL, Brown RH Jr, Constantine-Paton M, Bellingham MC (2008) Neonatal neuronal circuitry shows hyperexcitable disturbance in a mouse model of the adult-onset neurodegenerative disease amyotrophic lateral sclerosis. J Neurosci 28:10864–10874. CrossRef Medline

Vinsant S, Mansfield C, Jimenez-Moreno R, Del Gaizo Moore V, Yoshikawa M, Hampton TG, Prevette D, Caress J, Oppenheim RW, Milligan C (2013) Characterization of early pathogenesis in the SOD1(G93A) mouse model of ALS: part II, results and discussion. Brain Behav 3:431–457. CrossRef Medline

Vucic S, Nicholson GA, Kiernan MC (2008) Cortical hyperexcitability may precede the onset of familial amyotrophic lateral sclerosis. Brain 131:1540–1550. CrossRef Medline

Vucic S, Cheah BC, Yiannikas C, Kiernan MC (2011) Cortical excitability distinguishes ALS from mimic disorders. Clin Neurophysiol 122:1860–1866. CrossRef Medline

Yu X, Zuo Y (2011) Spine plasticity in the motor cortex. Curr Opin Neurobiol 21:169–174. CrossRef Medline